A study of the Group 1 metal tetra-aza macrocyclic complexes $[M(Me_4cyclen)(L)]^+$ using electronic structure calculations

Hanusha Bhakhoa,[1] Lydia Rhyman,[1,2,3] Edmond P. Lee,[4,5] Ponnadurai Ramasami[1,2*] and John M. Dyke[4*]

[1]Computational Chemistry Group, Department of Chemistry, University of Mauritius, Réduit 80837, Mauritius
[2]Department of Applied Chemistry, University of Johannesburg, Doornfontein 2028, South Africa
[3]Department of Chemistry, University of Johannesburg, PO Box 524, Auckland Park, Johannesburg 2006, South Africa
[4]School of Chemistry, University of Southampton, Southampton SO17 1BJ, UK
[5]Department of Applied Biology and Chemical Technology, The Hong Kong Polytechnic University, Hung Hom, Kowloon, Hong Kong

Corresponding Author(s)
*E-mail: ramchemi@intnet.mu (P.R.); jmdyke@soton.ac.uk (J.M.D.)

Graphical Abstract

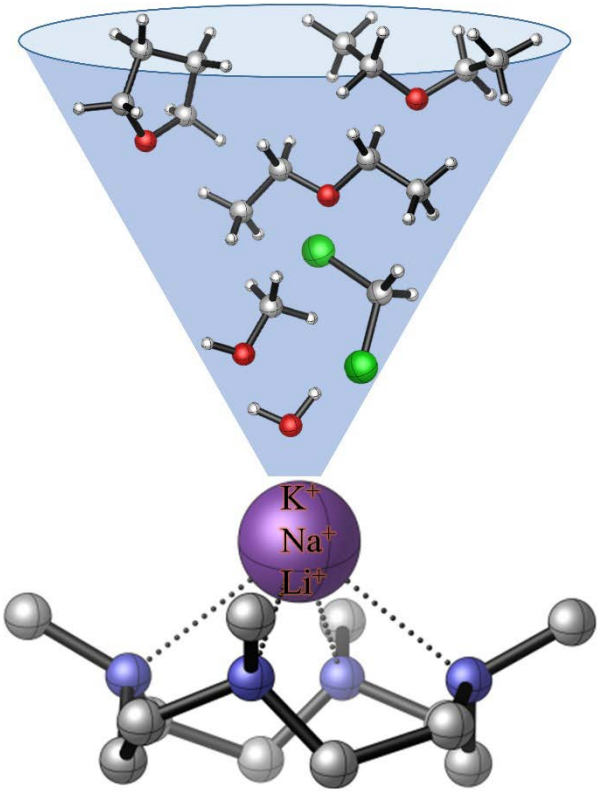

Abstract

Metal-cyclen complexes have a number of important applications. However, the coordination chemistry between metal ions and cyclen-based macrocycles is much less well studied compared to their metal ion-crown ether analogues. This work, which makes a contribution to address this imbalance by studying complex ions of the type $[M(Me_4cyclen)(L)]^+$, was initiated by results of an experimental study which prepared some Group 1 metal cyclen complexes, namely $[Li(Me_4cyclen)(H_2O)][BAr^F]$ and $[Na(Me_4cyclen)(THF)][BAr^F]$ and obtained their X-ray crystal structures [Dalton Trans., 2015, 44, 13853-13866].

The lowest $[M(Me_4cyclen)(L)]^+$ minimum energy structures (M = Li, Na, K, and L = H_2O, THF, DEE, MeOH, DCM) are studied using the BP86/6-311G(d,p) and B3LYP/6-311G(d,p) methods. The geometry of the $[M(Me_4cyclen)(L)]^+$ structures and, in particular, the conformation of L are found to be mainly governed by steric hindrance which decreases as the size of the ionic radii increases from $Li^+ \rightarrow Na^+ \rightarrow K^+$. Good correlation of computed geometrical parameters of $[Li(Me_4cyclen)(H_2O)]^+$ and $[Na(Me_4cyclen)(THF)]^+$ and geometrical parameters derived from their corresponding crystal structures $[Li(Me_4cyclen)(H_2O)]^+[BAr^F]^-$ and $[Na(Me_4cyclen)(THF)]^+[BAr^F]^-$ is obtained. Bonding analysis indicates that the stability of the $[M(Me_4cyclen)(L)]^+$ structures originates mainly from ionic interaction between the Me_4cyclen/L ligands and the M^+ centers. Accurate and consistent bond dissociation energies (BDEs) for the loss of L from $[M(Me_4cyclen)(L)]^+$ were obtained from single-point DF-LCCSD(T) and explicitly correlated DF-LCCSD(T)-F12x calculations. The DCM ligand is the least strongly bound to the M^+ centres in $[M(Me_4cyclen)(L)]^+$ compared to the *O*-donor solvent ligands studied as indicated by its lowest BDE values. The interaction between THF and $[M(Me_4cyclen)]^+$ is the strongest for M = Li and Na, with DEE competing with THF when M = K. The BDEs for the loss of L are lowest for the K^+ complexes. Also, infrared spectra of the $[M(Me_4cyclen)(L)]^+$ ions for M = Li, Na, K and L = H_2O, THF, DEE, MeOH, DCM have been computed.

The results indicate that the number and type of ligands, play a key role in stabilising the $[M(Me_4cyclen)]^+$ complexes and it is hoped that this work will encourage experimentalists to prepare and characterise $[M(Me_4cyclen)(L)]^+$ complexes.

Keywords

DFT, alkali metal, Me_4cyclen, bond dissociation energy, DF-LCCSD(T)-F12

1.0 Introduction

Alkali metal ions (Li^+, Na^+, K^+, Rb^+, and Cs^+) are prevalent in various aspects of life on earth, in the oceans, and within biological systems.[1-3] Since the early work of Pederson in the 1960's, the selective detection and uptake of alkali metal ions by *O*-donor macrocyclic hosts, such as crown ethers, are well established.[4] Although the alkali metal-crown ether combination has innumerable applications, the quest for host-guest systems with novel or advanced properties and functions is on-going.[5-8] 1,4,7,10-Tetraazacyclododecane, cyclen **1a** (Scheme 1), is one of the smallest *N*-donor analogues of crown ether, which can be easily derivatised by *N*-ligating sidearm groups.[9] Its usefulness in molecular sensing, catalysis, chirality signaling, and biomedicine, has made cyclen derivatives attractive alternative hosts to crown ethers.[10-14] However, the coordination chemistry between alkali metal ions and cyclen-based macrocycles[10,15-23] is less well studied compared to their crown ether analogues.

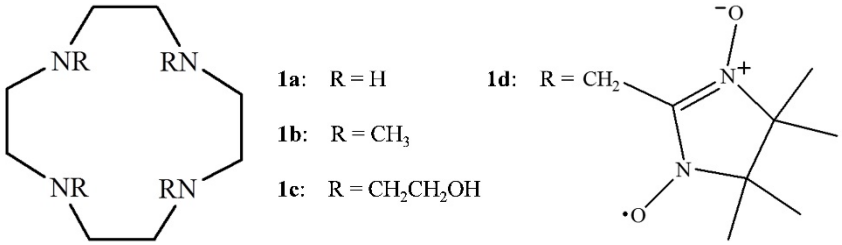

Scheme 1: Cyclen **1a** and some *N*-functionalised analogues **1b-d**.

Recently, as part of a study of a group of aza-macrocycles of Group 1 metal cations, some of us[22] reported the synthesis as well as the NMR and X-ray characterisation of the Li^+ and Na^+ complexes of 1,4,7,10-tetramethyl-1,4,7,10-tetraazacyclcododecane, Me_4cyclen **1b** (Scheme 1), namely [Li(Me_4cyclen)(H_2O)][BAr^F] and [Na(Me_4cyclen)(THF)][BAr^F] (THF = tetrahydrofuran; BAr^F = tetrakis{3,5-bis(trifluoromethyl)phenyl}borate). The crystal structures show a five coordinate square pyramidal cation, consisting of four *N*-atoms from the tetradentate macrocycle and one apical *O*-donor ligand, where the auxiliary *O*-donor ligands H_2O and THF occupy one of the exposed coordination sites of the metal centre above the macrocycle. However, attempts to synthesise the corresponding K^+, Rb^+, and Cs^+ complexes failed and resulted in the formation of [Me_4cyclenH][BAr^F]. This was an

unexpected outcome although K^+ complexes of cyclen derivatives **1c** and **1d** (Scheme 1) have been synthesised.[15,16]

We were intrigued by the successful syntheses of the Li^+ and Na^+ complexes of Me_4cyclen[22] but the unsuccessful synthesis of a K^+-Me_4cyclen complex, and this motivated us to look into possible factors which influence the formation and stability of alkali metal complexes of Me_4cyclen. Further, recent literature highlights the point that successful preparation and isolation of metal complexes can be attributed to the presence of residual coordinating solvents which can impart significant stability to the structure.[24] In this context, it is unclear how the nature of the ligand (L) coordinated above the metal in the $[M(Me_4cyclen)]^+$ cation contributes to the overall stability of the complex $[M(Me_4cyclen)(L)]^+$. In this work, the formation and stability of $[M(Me_4cyclen)(L)]^+$ is investigated using density functional theory (DFT) calculations, by studying the effect of coordinating commonly used *O*-donor solvents, namely H_2O, THF, diethyl ether (DEE), and methanol (MeOH) to $[M(Me_4cyclen)]^+$ (M = Li, Na, K). The fact that weakly coordinating polar dichloromethane (DCM) was used as a solvent during the successful syntheses of Li^+ and Na^+ complexes,[22] encouraged us to include L = DCM in this study.

As part of this investigation, the dissociation energy of the ligand (L) from each $[M(Me_4cyclen)(L)]^+$ ion was computed using DFT calculations for M = Li, Na, K, and L = H_2O, THF, DEE, MeOH, DCM. Then, improved dissociation energies were obtained using single-point DF-LCCSD(T)[25] and explicitly correlated DF-LCCSD(T)-F12[26] calculations.[23,27,28] Additionally, geometrical parameters and infrared (IR) spectra were computed. These should be useful in identifying $[M(Me_4cyclen)(L)]^+$ compounds, if in the future they are synthesised ideally in crystalline form.

2.0 Computational Details

The DFT functionals BP86[29] and B3LYP[30] were used to perform geometry optimisations for all the chemical species investigated in this work.[31,32] The 6-311G(d,p) basis set[33] was employed for the atoms H, C, N, O, Cl, Li, Na, and K. The functionals were selected, with the 6-311G(d,p) basis set, based on results of our recent studies on alkali metal ion-macrocyclic complexes.[22,23,34] Geometry optimisation was followed by analytic Hessian computation at the same levels of theory, and the absence of negative Hessian eigenvalues confirmed the stationary points as minima on the potential energy hypersurfaces. Bond dissociation energies (BDEs) were calculated for the process, $[M(Me_4cyclen)(L)]^+ \rightarrow [M(Me_4cyclen)]^+ + L$, where M = Li, Na, K, and L = H_2O, THF, DEE, MeOH, DCM, using these functionals with the 6-311G(d,p) basis set.[35] Basis set superposition error (BSSE) correction, as implemented by the Boys-Bernardi counterpoise method,[36] and zero-point energy (ZPE) correction were included in the BDEs. Reported relative energies are given at 298.15 K and 1 atm. All density functional computations were performed using the Gaussian 09 package.[37] Natural bond orbital (NBO) analysis[38,39] was also carried out using the NBO program as implemented in the Gaussian 09 package.[40] Throughout this work, $[M(Me_4cyclen)(L)]^+$ structures optimised with the BP86 functional are denoted **M-L-1a** and those optimised with the B3LYP functional are denoted **M-L-2a**.

High level *ab initio* methods were employed to assess the performance of the DFT calculations and to obtain more reliable BDEs.[23,27,28] Single-point DF-LCCSD(T)[25] and explicitly correlated DF-LCCSD(T)-F12x (x = a, b)[26] calculations were performed at the BP86/6-311G(d,p) and B3LYP/6-311G(d,p) lowest minimum energy geometries of $[M(Me_4cyclen)(L)]^+$, $[M(Me_4cyclen)]^+$, and L in the above dissociation process using the MOLPRO 2015.1 program.[41] All DF-LCCSD(T) and DF-LCCSD(T)-F12x calculations were preceded by a density fitted Hartree-Fock (HF) calculation.[42] The local correlation methods together with the density fitting (DF) approximation allow the efficient treatment of larger molecules. The inclusion of explicitly correlated terms accounts for basis set incompleteness and domain approximation associated errors.[25,26] The first step in the DF-LCCSD(T)-F12x calculations involves DF-LMP2-F12 calculations which were performed using the 3*A ansatz approximation as detailed in references 43 and 44. Two sets of ansatz options, namely (Loc,Fix) and (Fix,NoX) were used, the former being the default for DF-LCCSD(T)-F12x

calculations.[43-45] The (Fix,NoX) ansatz option was used to avoid unreasonable BDE values obtained with the (Loc,Fix) option for calculations involving chlorine atoms (*i.e.* in calculations with L = DCM) (*vide infra*).

In the DF-LCCSD(T) calculations, the aug-cc-pVDZ atomic orbital (AO) basis set[46-48] was employed in conjunction with the aug-cc-pVDZ/MP2FIT[49,50] and aug-cc-pVDZ/JKFIT auxiliary basis sets (ABS)[51,52] for the H, C, N, O, and Cl atoms. The corresponding DF-LCCSD(T)-F12x calculation uses cc-pVDZ-F12 as the AO basis set[53] and cc-pVDZ-F12/OPTRI as the complementary auxiliary basis set (CABS).[54] For Li/Na, the aug-cc-pwCVDZ[55] and cc-pCVDZ-F12[56] AO basis sets were used in the DF-LCCSD(T) and DF-LCCSD(T)-F12x calculations, respectively. The aug-cc-pwCVDZ/MP2FIT[56] def2-QZVPP/JKFIT[57] and cc-pCVDZ-F12/OPTRI[56] basis sets were chosen as the ABS and the CABS, respectively. The 1s orbital on Li^+ and the 2s and 2p orbitals on Na^+ were considered to be valence as in our previous work.[23] The double-ζ quality basis sets used in the DF-LCCSD(T) and DF-LCCSD(T)-F12x calculations are denoted in the text as DZ and DZ-F12, respectively.

High level single-point calculations with the aug-cc-pVTZ basis set[46-49,51,52] on the complexes studied, which consist of a maximum of 60 atoms, failed because the maximum CPU time allowed was exceeded. Thus, the def2-TZVPP basis set,[58] which is slightly smaller (with respect to the aug-cc-p-VTZ basis set) but is a well-balanced triple-ζ AO basis set,[59] was used along with the associated default ABS (def2-TZVPP/MP2FIT[60-62] and def2-TZVPP/JKFIT)[57] and/or the CABS (def2-TZVPP/OPTRI)[63] for the H, C, N, O, and Cl atoms. Def2-TZVPP was employed as the triple-ζ AO basis set for Li and Na.[58] In the DF-LCCSD(T) calculation, the def2-TZVPP AO basis set was augmented with the following uncontracted functions, namely, two s (ζ = 5.0134, 1.6427), two p (ζ = 4.2222, 0.93), and one d (ζ = 0.85) for Li and two s (ζ = 4.2353, 0.6984), two p (ζ = 1.1907, 0.3846), two d (ζ = 3.4561, 0.7449), and one f (ζ = 3.227) for Na. In the DF-LCCSD(T)-F12x calculation, the def2-TZVPP AO basis set was augmented with a set of spd(f) functions, with exponents of ζ_s = 0.406129, ζ_p = 1.37526, and ζ_d = 4.518674 for Li and ζ_s = 3.764945, ζ_p = 3.0511, ζ_d = 5.420585, and ζ_f = 4.557524 for Na. These additional uncontracted basis functions account for core-correlation and were obtained by analysing and comparing the range of the exponents of the corresponding cc-pVTZ[55] (cc-pVTZ-F12)[56] and aug-cc-pwCVTZ[55] (cc-

pCVTZ-F12)[56] AO basis sets. Def2-QZVPP/MP2FIT[50] and def2-QZVPP/JKFIT[57] were selected as fitting basis sets and cc-pCVTZ-F12/OPTRI was selected as the CABS.[56] The triple-ζ quality basis sets used in the DF-LCCSD(T) and DF-LCCSD(T)-F12x calculations are denoted in the text as TZ and TZ-F12, respectively.

For K, the ECP10MDF effective core potential (ECP) was employed to account for the 1s, 2s, and 2p orbitals, where MDF indicates that the neutral atom is used in the derivation of the ECP which involves the use of the fully relativistic approach as described by the Stuttgart/Cologne group.[64,65] The atomic basis set for the K^+ $3s^2$ $3p^6$ orbitals was designed to couple with the ECP10MDF ECP as follows:- An even-tempered (11s9p) set of functions were contracted to [1s1p] with the coefficients for the K^+ $3s^2$ $3p^6$ occupied atomic orbitals being obtained from a restricted Hartree-Fock (RHF) calculation on K^+ using the ECP10MDF ECP and the (11s9p) basis set. Both the exponents of the 11s and 9p primitive functions were centered on ζ = 1.2 with a ratio of 2.0. Additional uncontracted functions, namely, three s (ζ = 1.125, 0.45, 0.18), two p (ζ = 0.8, 0.32), and two d (ζ = 0.6, 0.24), were added to give the ECP10MDF[4s3p2d] basis set which is of the same standard as the aug-cc-pVDZ basis set. Four s (ζ = 2.8125, 1.125, 0.45, 0.18), two p (ζ = 1.1, 0.15), two d (ζ = 1.2, 0.4), and one f (ζ = 0.6) uncontracted functions were incorporated to yield the ECP10MDF[5s3p2d1f] basis set which is of approximately triple-ζ quality. For K, the def2-QZVPP basis set was used as both the ABS and the CABS.[50,57,63]

All computations were carried out with resources (CPU time and software) provided by the GridChem Science Gateway[66-68] and the UK National Service for Computational Chemistry Software (NSCCS).

3.0 Results and Discussion

3.1 Geometrical parameters

3.1a Metal-cyclen 1b structures (see scheme 1)

$[M(Me_4cyclen)]^+$ and $[M(Me_4cyclen)(L)]^+$

Initially, the alkali metal-Me_4cyclen complexes, $[M(Me_4cyclen)]^+$ (M = Li, Na, and K), were optimised in the C_4(++++) conformation using the DFT BP86/6-311G(d,p) and B3LYP/6-311G(d,p) methods. In C_4(++++), C_4 corresponds to the symmetry of the complexes and (++++) indicates that all four *N*-donor atoms of the Me_4cyclen ring lie in the same plane and orient towards the M^+ center. It should be noted that C_4(++++) is the most frequently found conformation in X-ray structures and geometry optimisation calculations of $[M(Me_4cyclen)]^+$ complexes and their derivatives, with minor variations being observed in the symmetry of some complexes.[10,15-23] The BP86 minimum energy structures in the C_4(++++) conformation are shown in Figure 1. Very similar geometrical parameters were obtained with both the BP86 and B3LYP functionals (see Table S1). The $[M(Me_4cyclen)]^+$ structures obtained were then used as initial geometries in the full optimisation of the $[M(Me_4cyclen)(L)]^+$ structures. The exposed M^+ centre of each $[M(Me_4cyclen)]^+$ optimised structure allows the possibility for additional ligand coordination. Thus, the *O*- or *Cl*-donor atoms of the H_2O, THF, DEE, MeOH, and DCM ligands can interact with the M^+ centres at the apical position of the $[M(Me_4cyclen)]^+$ backbone forming pseudo-square pyramidal $[M(Me_4cyclen)(L)]^+$ structures. The BP86 and B3LYP lowest $[M(Me_4cyclen)(L)]^+$ minimum energy structures are denoted as **M-L-1a** (Figure 2) and **M-L-2a** (Figure S1), respectively (M = Li, Na, K, and L = H_2O, THF, DEE, MeOH, DCM). Several $[M(Me_4cyclen)(L)]^+$ low-lying structures are provided in Figures S2-S7. The symmetries of the BP86 and B3LYP lowest minimum energy structures for each $[M(Me_4cyclen)(L)]^+$ complex are the same for each metal, except for **Na-DCM-1a** and **Na-DCM-2a** (C_1 and C_2, respectively) and **K-DEE-1a** and **K-DEE-2a** (C_2 and C_1, respectively). The $[M(Me_4cyclen)(L)]^+$ structures obtained are slightly sensitive to the functionals employed with the main difference, notably between the **M-L-1a** (BP86) and **M-L-2a** (B3LYP) lowest minimum energy structures, lying in the spatial arrangement of L. For example, the dihedral angles, *Ø*(N1–M–O–H1) of the **Na-H_2O-1a** (Figure 2) and **Na-H_2O-2a** (Figure S1) structures are 55.3° and 14.7°, respectively. However, it is noteworthy that rotation about the M–O (H_2O, THF, DEE, MeOH) and M–Cl (DCM) axis entails negligible change in the relative energy of the resulting

$[M(Me_4cyclen)(L)]^+$ structures, suggesting a very flat rotational potential with a low rotational barrier [see Further Information in Supplementary Information (SI)].

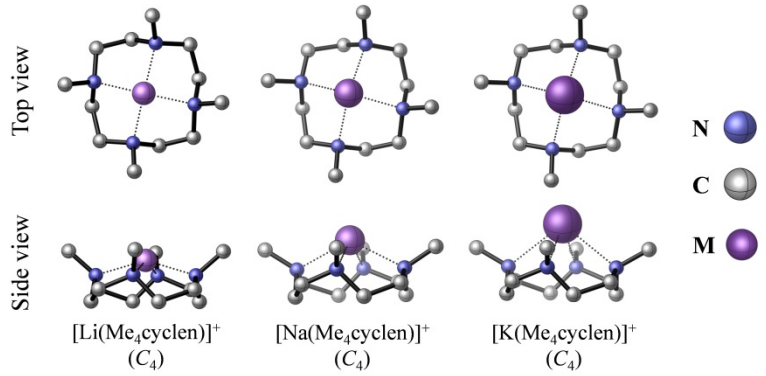

Figure 1: Optimised lowest energy structures of $[M(Me_4cyclen)]^+$ obtained using the BP86/6-311G(d,p) method. The symmetry of each structure is provided. All H atoms are omitted for clarity.

Complexation of $[M(Me_4cyclen)]^+$ to L results in the **M-L-1a** (BP86) and the **M-L-2a** (B3LYP) minimum energy structures having either a C_2(++++) or a C_1(++++) conformation. Selected geometrical parameters of the structures **M-L-1a** (**M-L-2a)** are provided in Tables 1(a), 1(b), S2, and S3 and these are compared with those of the $[M(Me_4cyclen)]^+$ optimised structures in Table S1. Upon complexation, the Li–N, Na–N, and K–N bond distances lengthen by 0.007-0.156 Å (BP86; B3LYP, 0.020-0.210 Å), 0.016-0.075 Å (BP86; B3LYP, 0.026-0.068 Å), and 0.017-0.056 Å (BP86; B3LYP, 0.018-0.058 Å), respectively. A decrease of less than 5° in the N–M–N bond angles is observed along with an increase of about 0.030-0.300 Å (BP86; B3LYP, 0.040-0.320 Å) in the distance between the plane of the four *N*-donor atoms of the Me_4cyclen ring and the M^+ ions. The cavity size of the Me_4cyclen ring expands on addition of L to Me_4cyclen by a maximum of 0.231 A^2 (BP86; B3LYP, 0.276 A^2) for the Li^+ complexes in the order of **Li-DEE-1a** (**Li-DEE-2a**) > **Li-THF-1a** (**Li-THF-2a**) > **Li-MeOH-1a** (**Li-MeOH-2a**) > **Li-H_2O-1a** (**Li-H_2O-2a**) > **Li-DCM-1a** (**Li-DCM-2a**). The change in the cavity size of the Me_4cyclen ring for the Na^+ and K^+ lowest minimum energy structures is negligible (≤ 0.030 A^2). In fact, as the size of the ionic radii of M^+ increases from Li^+ (0.92 Å) → Na^+ (1.24 Å) → K^+ (1.55 Å),[69] the geometrical parameters associated with the $[M(Me_4cyclen)]^+$ fragment in $[M(Me_4cyclen)(L)]^+$ become closer to those of their $[M(Me_4cyclen)]^+$ parent structure.

Complexation with the DCM ligand affects the geometrical parameters of [M(Me$_4$cyclen)]$^+$ backbone to a lesser extent than complexation with *O*-donor ligands.

.

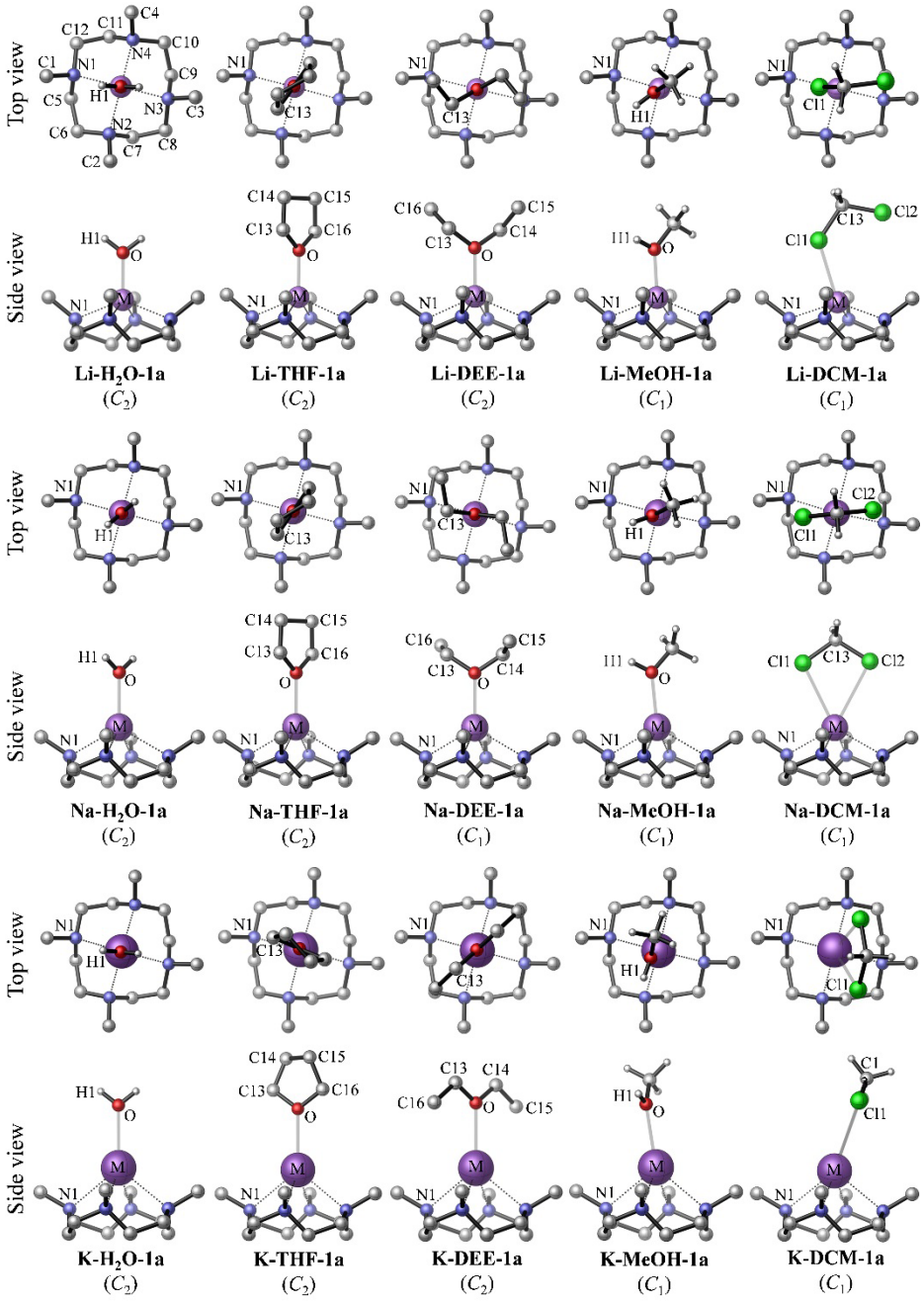

Figure 2: Lowest [M(Me$_4$cyclen)(L)]$^+$ minimum energy structures obtained using the BP86/6-311G(d,p) method. The symmetry of each structure is provided. Selected H atoms are omitted for clarity.

The M–N bond distances, N–M–N bond angles, N–C–C–N dihedral angles, the cavity size of the Me_4cyclen ring, and the distance between the plane formed by the four *N*-donor atoms of the Me_4cyclen ring and the M^+ ions, for the **M-L-1a** (**M-L-2a**) structures follow similar trends as their $[M(Me_4cyclen)]^+$ counterparts as the size of the ionic radii of M^+ increases from Li^+ to Na^+ to K^+.

The overall changes observed in the geometrical parameters upon complexation of $[M(Me_4cyclen)]^+$ to L indicate that (i) the effects of steric hindrance between Me_4cyclen and L are maximum in **Li-DEE-1a** (**Li-DEE-2a**), (ii) DCM coordinates weakly to the $[M(Me_4cyclen)]^+$ unit as compared to its *O*-donor analogues, and (iii) as the size of the ionic radii of M^+ increases from $Li^+ \rightarrow Na^+ \rightarrow K^+$, steric hindrance between Me_4cyclen and L in **M-L-1a** (**M-L-2a**) decreases, and thus the effect on the geometry of the $[M(Me_4cyclen)]^+$ unit in $[M(Me_4cyclen)(L)]^+$ also decreases

An analysis of the lowest minimum energy structures with *O*-donor ligands reveals that the M–O bond of **M-L-1a** (**M-L-2a**), for L = H_2O, THF, and DEE, is essentially normal to the plane formed by the four *N*-donor atoms of Me_4cyclen, with the dipole moment of each structure aligning along the M–O bond. The M–O bond of **M-MeOH-1a** (**M-MeOH-2a**) is tilted by ≈ 3-10° from the normal of the equatorial plane. In general, the M–O bond distances of **M-H_2O-1a** (**M-H_2O-2a**), **M-THF-1a** (**M-THF-2a**), **M-DEE-1a** (**M-DEE-2a**), and **M-MeOH-1a** (**M-MeOH-2a**) are comparable (for M = Li and Na; see Tables 1 and S2). The K–O bond distance of **K-DEE-1a** (BP86, 2.805 Å; B3LYP, 2.788 Å) is significantly longer than the K–O bonds in **K-H_2O-1a** (BP86, 2.718 Å; B3LYP, 2.711 Å), **K-THF-1a** (BP86, 2.721 Å; B3LYP, 2.705 Å), and **K-MeOH-1a** (BP86, 2.729 Å; B3LYP, 2.713 Å). This observation can be correlated to the spatial arrangement of the DEE fragment in the complexes. The **M-DEE-1a** (**M-DEE-2a**) structures (for M = Li and Na) have their DEE fragment in a gauche-gauche (GG) conformation while for M = K, **K-DEE-1a** (**K-DEE-2a**) adopts a trans-trans (TT) conformation. The M–N and M–O bond distances of **K-DEE-1a** (**K-DEE-2a**) are longer than their Li^+ and Na^+ counterparts, thus its DEE framework is free to adopt a less sterically hindered conformation, a TT conformation. This is consistent with the known lowest energy structure of DEE in the gas-phase which is known to be TT[70,71] and the results of DFT BP86 and B3LYP calculations on DEE summarised in Figures S8 and S9 (Figure S9 shows a diagram of the TT, TG, and GG structures of DEE).

Table 1 (a): Selected geometrical parameters of the lowest $[M(Me_4cyclen)(L)]^+$ minimum energy structures obtained using the BP86/6-311G(d,p) method for M = Li, Na, and K with L = H_2O and THF.

	M-H_2O-1a				**M-THF-1a**			
Bond distances (Å)	Li	Expt.[a]	Na	K	Li	Na	Expt.[a]	K
M–N1	2.256	2.186(8)	2.502	2.842	2.253	2.521	2.463(4)	2.853
M–N2	2.254	2.206(8)	2.505	2.835	2.330	2.522	2.461(3)	2.843
M–N3	2.256	2.179(8)	2.502	2.842	2.253	2.521	2.453(4)	2.853
M–N4	2.254	2.154(9)	2.505	2.835	2.330	2.522	2.444(4)	2.843
M–O	2.009	1.98(1)	2.340	2.718	2.028	2.351	2.244(3)	2.721
Bond angles (°)								
N1–M–N2	82.3	82.8(3)	75.9	66.9	80.9	75.3	75.4(1)	66.8
N2–M–N3	82.4	82.1(3)	76.2	66.9	81.6	75.6	75.6(1)	66.7
N3–M–N4	82.3	84.7(3)	75.9	66.9	80.9	75.3	76.0(1)	66.8
N4–M–N1	82.4	82.6(3)	76.2	66.9	81.6	75.6	75.5(2)	66.7
Torsion (°)								
N1–C5–C6–N2	-57.1	59.4(7)	-61.9	-64.7	-56.1	-62.2	-64(1)	-64.9
N2–C7–C8–N3	-57.1	55.8(8)	-62.6	-64.2	-59.9	-62.7	-61(1)	-64.4
N3–C9–C10–N4	-57.1	54.0(9)	-61.9	-64.7	-56.1	-62.2	-59(1)	-64.9
N4–C11–C12–N1	-57.1	57.5(7)	-62.6	-64.2	-59.9	-62.7	-65(1)	-64.4
N1–M–O–H1	11.7	–	55.3	10.1	–	–	–	–
N1–M–O–C13	–	–	–	–	69.1	70.0	59.6	-7.7

[a] Corresponds to the $[Li(Me_4cyclen)(H_2O)]^+$ and $[Na(Me_4cyclen)(THF)]^+$ crystal structures, respectively.[22]

In order to provide further insight into the structure of L in the lowest $[M(Me_4cyclen)(L)]^+$ minimum energy structures, BP86 and B3LYP calculations were performed on the monosolvated alkali metal ion structures, $[M^+\text{-L}]$ (M = Li, Na, K, and L = H_2O, THF, DEE, MeOH, DCM) (see Further Information in the SI). For L = DEE, all the lowest $[M^+\text{-DEE}]$ minimum energy structures have their DEE fragment in the TT conformation with the GG conformation being 15.8 (16.8), 14.2 (15.9), and 9.6 (11.3) $kJ.mol^{-1}$ higher in energy for M = Li, Na, and K, respectively (Figure S8) (BP86 values are quoted with B3LYP values in brackets).

In the $[M(Me_4cyclen)(L)]^+$ complexes with L = DEE, for M = Li and Na, it appears that the close proximity between the Me_4cyclen and DEE forces DEE to adopt a more

sterically hindered conformation in the **M-DEE-1a** (**M-DEE-2a**) structures than in the M = K case. Further, a significant decrease of ≈ 20° in the dihedral angles $Ø_1$(C14–O–C13–C16) and $Ø_2$(C13–O–C14–C15) is observed arising from steric hindrance on going from **Na-DEE-1a (Na-DEE-2a)** to **Li-DEE-1a** (**Li-DEE-2a**) which is accompanied by a decrease in the corresponding M–N and M–O bond distances. In contrast, for the corresponding [M^+-L] structures for M = Li and Na, the dihedral angles $Ø_1$ and $Ø_2$ of the least stable [Li^+-DEE] (GG) structure [BP86, 84.6°; B3LYP, 85.3°] are comparable to that of [Na^+-DEE] (GG) [BP86, 85.9°; B3LYP, 86.7°].

The **M-DCM-1a** (**M-DCM-2a**) [M(Me_4cyclen)(L)]$^+$ structures (M = Li, Na, K) differ significantly from each other. The small Li^+ ion in **M-DCM-1a** (**M-DCM-2a**) interacts with DCM in a monodentate η^1-Cl1 coordination mode with the Li–Cl2 distance (BP86, 4.344; B3LYP, 4.405 Å) being significantly greater than the sum of the van der Waals (vdW) radii of the Li (1.81 Å) and Cl (1.75 Å) atoms.[72] On the other hand, Na^+ and K^+ ions interact with DCM in a bidentate η^2-Cl1,Cl2 coordination mode with their M–Cl distances being within the sum of their respective vdW contact distances.[72] Comparison of the [M^+-DCM] (M = Li, Na, K) structures (Figure S8), where M^+ coordinates to DCM in an η^2-Cl,Cl fashion, highlights the presence of steric hindrance between Me_4cyclen and DCM in **Li-DCM-1a** (**Li-DCM-2a**). Further, the plane in DCM defined by Cl1–C13–Cl2 in **Na-DCM-1a** (**Na-DCM-2a**) is perpendicular to the plane of the four *N*-donor atoms of the Me_4cyclen ring while that of the K^+ analogue deviates from perpendicular. This implies that the tilted DCM fragment in the **K-DCM-1a** (**K-DCM-2a**) structures is less sterically hindered by the methyl groups of the Me_4cyclen macrocycle than in the Na^+ case.

The **Li-H_2O-1a** (**Li-H_2O-2a**) and **Na-THF-1a** (**Na-THF-2a**) computed geometrical parameters are compared with their corresponding [Li(Me_4cyclen)(H_2O)]$^+$ and [Na(Me_4cyclen)(THF)]$^+$ geometrical parameters obtained from the crystal structures[22] in Table 1(a). In general, the agreement between computed and exprimental parameters is good. The BP86 M–N bond lengths are all slightly higher and the BP86 N–M–N bond angles are all slightly lower than the experimental values. This is also true of the B3LYP computed geometrical parameters. In general, the computed and experimentally derived structures are comparable with differences of < 0.110 Å in M–N bond distances, < 2.5° in N–M–N bond angles, and < 3.5° in N–C–C–N dihedral angles [Table 1(a)].

$[Li(Me_4cyclen)(H_2O)]^+$ and $[Na(Me_4cyclen)(THF)]^+$ are the two $[M(Me_4cyclen)(L)]^+$ ions for which X-ray crystal structures have been obtained.[22] $[Li(Me_4cyclen)(H_2O)][BAr^F]$ was prepared by reaction of $[Li(H_2O)_4][BAr^F]$ with Me_4cyclen in DCM. Similarly, reaction of Me_4cyclen with $Na[BAr^F].2THF$ in DCM yielded $[Na(Me_4cyclen)(THF)][BAr^F]$. Clearly, the presence of H_2O or THF in the crystal structures arises from the $[Li(H_2O)_4][BAr^F]$ and $Na[BAr^F].2THF$ salts used, respectively. It is noteworthy that no evidence of coordination of DCM (or *n*-hexane, the other solvent used in these syntheses) to the $[M(Me_4cyclen)]^+$ ion was observed. Also, attempts to synthesise the $[M(Me_4cyclen)(L)][BAr^F]$ salts for M = K, Rb, and Cs were unsuccessful resulting only in isolation of $[Me_4cyclenH][BAr^F]$.[22]

3.1b Metal-cyclen 1c,1d structures (see scheme 1) $[M(Me_4cyclen)(L)]^+$

Only two other related crystal structures are available in the literature and these are crystal structures of $[K(cyclen)(L)]^+$ complexes.[15,16] Both consist of an octa-coordinated K^+ structure with four *N*-donor atoms from the cyclen backbone and four *O*-donor atoms derived (i) from four 2-hydroxyethyl groups (Scheme 1, **1c**) and (ii) from four 4,4,5,5-tetramethylimidazolin-1-oxyl-3-oxide-CH_2 groups (Scheme 1, **1d**) (see Figure S10). These structures are denoted K^+-**1c** and K^+-**1d**. DFT geometry optimisation calculations were also performed on these cations with the BP86 and B3LYP functionals. Good correlation of the computed geometrical parameters with the corresponding parameters obtained from the crystal structures was obtained (Table S6). The M–N bond distances as well as the distance between the basal plane of the four *N*-donor atoms and the K^+ ion of both optimised structures are longer while their N–M–N bond angles are smaller than that of **K-L-1a** (**K-L-2a**). In K^+-**1c** and K^+-**1d**, the M–O bond distances are shorter than the corresponding M–N distances. This was also observed for the **K-L-1a** (**K-L-2a**) structures, as well as for the other **M-L-1a** (**M-L-2a**) structures, where M = Li, Na, and L = H_2O, THF, DEE, MeOH. This is consistent with the higher affinity of *O*-donor ligands towards alkali metal ions than the *N*-donor ligands. Also, a comparison of the computed geometrical parameters of **K-L-1a** (**K-L-2a**) and K^+-**1c**/K^+-**1d** with those of the parent $[K(Me_4cyclen)]^+$ complex shows that the effect of coordinating one instead of four *O*-donor ligands to the K^+ centre is moderate but significant. For example, using BP86 computed values, the K–N bonds in K^+-**1c** are ~ 0.08 Å longer and the K–N bonds in K^+-**1d** are ~ 0.16 Å longer than the **K-L-1a** values. The K–O bonds in K^+-**1c** and K^+-**1d** are also longer than the one K–O bond in each of the **K-L-1a** complexes by ~

373 0.10 Å. Clearly, the number and type of *O*-donor ligands will play an important role in
374 determining the stability of the K^+ complexes of cyclen derivatives.

375

376 Table 1(b): Selected geometrical parameters of the lowest $[M(Me_4cyclen)(L)]^+$ minimum
377 energy structures obtained using the BP86/6-311G(d,p) method, for M = Li, Na, and K with
378 L = DEE, MeOH, and DCM.

	M-DEE-1a			**M-MeOH-1a**			**M-DCM-1a**		
Bond distances (Å)	Li	Na	K	Li	Na	K	Li	Na	K
M–N1	2.329	2.529	2.851	2.266	2.500	2.842	2.260	2.504	2.831
M–N2	2.271	2.515	2.862	2.269	2.509	2.840	2.190	2.484	2.824
M–N3	2.329	2.533	2.851	2.258	2.511	2.843	2.228	2.506	2.822
M–N4	2.271	2.512	2.862	2.257	2.511	2.844	2.180	2.474	2.823
M–O	2.042	2.364	2.805	2.016	2.354	2.729	–	–	–
M–Cl1	–	–	–	–	–	–	2.784	3.188	3.623
M–Cl2	–	–	–	–	–	–	4.344	3.369	3.626
Bond angles (°)									
N1–M–N2	81.0	75.5	66.5	81.5	75.9	66.9	83.9	76.5	67.3
N2–M–N3	81.1	75.4	66.6	82.4	76.0	66.8	83.9	76.4	67.3
N3–M–N4	81.0	75.4	66.5	82.2	75.7	66.9	84.5	76.7	67.3
N4–M–N1	81.1	75.4	66.6	82.4	76.0	66.9	83.8	76.6	67.3
Torsion (°)									
N1–C5–C6–N2	-59.0	-63.0	-64.6	-56.6	-62.1	-64.8	-58.7	-62.9	-64.6
N2–C7–C8–N3	-57.8	-62.0	-65.6	-57.7	-62.3	-64.8	-55.2	-61.7	-64.6
N3–C9–C10–N4	-59.0	-63.0	-64.6	-57.2	-62.1	-64.7	-55.2	-63.1	-64.5
N4–C11–C12–N1	-57.8	-61.5	-65.6	-57.7	-62.2	-65.0	-55.7	-61.6	-64.9
N1–M–O–H1	–	–	–	50.6	31.4	82.5	–	–	–
N1–M–O–C13	43.2	8.5	57.7	–	–	–	–	–	–
N1–M–C13–Cl1	–	–	–	–	–	–	12.8	23.2	104.4

379

3.2 Bonding analysis

A reasonable description of the electronic structures of the **M-L-1a** (**M-L-2a**) $[M(Me_4cyclen)(L)]^+$ ions can be obtained from NBO analysis and from inspection of the converged wavefunctions. The natural charges on selected centres of the optimised (a) free Me_4cyclen and L ligands, (b) $[M(Me_4cyclen)]^+$, (c) $[M^+\text{-L}]$, and (d) **M-L-1a** (**M-L-2a**) structures are given in Tables S7-10.

Coordination of L to M^+ results in a slight drop of the positive charge on the cation (from +1.0). Taking the computed charge densities on M in $[M^+\text{-L}]$ for M = Na as examples, values obtained were +0.99, +0.98, +0.97, +0.98, and +0.94 for L = H_2O, THF, DEE, MeOH, and DCM (see Table S8). For the *O*-containing ligands, the charge on the O atom coordinated to the metal becomes more negative on forming $[M^+\text{-L}]$ in all cases. For example, in THF, the negative charge on the O atom increases from -0.57 in THF to -0.71 in $[Na^+\text{-THF}]$ (BP86 charge densities are quoted above but the B3LYP values are very similar). Also, the negative charges on the carbon atoms of the THF show virtually no change but the positive charges on the hydrogen atoms increase on going from THF to $[Na^+\text{-THF}]$. This is consistent with charge transfer taking place from the ligand O atom to the metal and then electron density being transferred to the O atom within the ligand via the σ O–C, σ C–C, and σ C–H bonding orbitals of THF. In the case of L = DCM, a similar picture holds with the charge on the carbon atom becoming less negative and the charge of the hydrogen atoms becoming more positive on forming $[M^+\text{-L}]$. Again on forming $[M^+\text{-L}]$, charge transfer occurs from Cl to M^+ accompanied by electron density transfer to the Cl atoms from within the ligand via the σ C–Cl and σ C–H bonding orbitals. For M = Na and K, where the metal is bonded to two chlorine atoms, the Cl atoms show a slight increase of negative charge whereas for M = Li, where the metal is bonded to one Cl atom, this Cl atom shows a slight decrease of negative charge on going from M^+ + L to $[M^+\text{-L}]$.

Coordination of M^+ to Me_4cyclen to give $[M(Me_4cyclen)]^+$ shows similar trends. The positive charge on the metal drops from +1.0 to +0.69, +0.79, and +0.87 for Li^+, Na^+, and K^+. Also the charge on the nitrogen atoms coordinated to the metal becomes more negative (see Table S7). Upon complexation of M^+ to Me_4cyclen, electron density is transferred from the N 2p non-bonding orbitals of the Me_4cyclen ring to the metal, with electron density then being transferred to the N atoms from the σ C–N, σ C–C, and σ C–H bonding orbitals. The

411 negative charges on the carbon atoms in Me_4cyclen show only small changes but the positive
412 charges on the hydrogen atoms of the CH_2 as well as the CH_3 units in the macrocycle
413 increase.

414 Addition of a solvent, L, to $[M(Me_4cyclen)]^+$ to give $[M(Me_4cyclen)(L)]^+$ gives rise
415 to further electron transfer to the metal and hence, a reduced metal positive charge. As
416 observed for the $M^+ + L \rightarrow [M^+\text{-}L]$ process, the negative charge on the O atom (of the *O*-
417 containing solvents) increases, the negative charges on the carbon atoms of the solvent show
418 only small changes and the positive charges on the H atoms of the solvent increase.
419 Electron transfer takes place from the O atom to the metal accompanied by electron transfer
420 to the O atom from the σ O–C, σ C–C, and σ C–H bonding orbitals of the ligand. Similar
421 trends are observed in the L = DCM case.

422 A comparison of the *O*-containing $[M^+\text{-}L]$ complexes shows that the O atoms of $[M^+\text{-}$
423 $H_2O]$ are the most negatively charged while its M^+ centres are the most positively charged
424 with natural charges in the order of $[M^+\text{-}H_2O] > [M^+\text{-}MeOH] > [M^+\text{-}THF] > [M^+\text{-}DEE]$. A
425 similar trend occurs for the corresponding **M-L-1a** (**M-L-2a**) structures, indicating less
426 electron density being transferred from H_2O to M^+ with respect to the THF, DEE, and MeOH
427 ligands, consistent with the known order of first adiabatic ligand ionisation energies of H_2O
428 > MeOH > THF > DEE.[72] More electron density is transferred from the Cl atoms to the M^+
429 centres in both the $[M^+\text{-}DCM]$ and **M-DCM-1a** (**M-DCM-2a**) structures than for the *O*-
430 containing solvents, as indicated by the lower positive charges on the M^+ centres for L =
431 DCM compared to that of the *O*-containing analogues. The lower electronegativity of the Cl
432 atom with respect to the O atom[74] is consistent with the higher transfer of electron density to
433 the M^+ centres. A similar observation has been made in a study of the bonding characters of
434 $[Ag^+\text{-}DCM]$ and $[Ag^+\text{-}OSO]$, where the DCM and SO_2 ligands interact with Ag^+ via bidentate
435 η^2-Cl,Cl and monodentate η^1-O coordination modes, respectively.[75]

436 On considering the steps $M^+ + Me_4cyclen \rightarrow [M(Me_4cyclen)]^+$ and $[M(Me_4cyclen)]^+$
437 $+ L \rightarrow [M(Me_4cyclen)(L)]^+$, significantly more electron density is transferred to the metal in
438 the first step than the second step. This implies that M^+ is more tightly bound to Me_4cyclen
439 than L in the **M-L-1a** (**M-L-2a**) $[M(Me_4cyclen)(L)]^+$ complexes. Also, the M^+ centres accept
440 less electron density as the size of the radii of the M^+ ions increases from $Li^+ \rightarrow Na^+ \rightarrow K^+$
441 and the first ionisation energy of M decreases from Li → Na → K. In general, the NBO

analysis indicates that the metal-ligand bonding in the [M(Me$_4$cyclen)]$^+$, [M$^+$-L], and **M-L-1a** (**M-L-2a**) [M(Me$_4$cyclen)(L)]$^+$ complexes is mainly ionic in nature.

3.3 Computed Infrared (IR) Spectra

Computed harmonic IR spectra together with selected vibrational modes for the [M$^+$-L], [M(Me$_4$cyclen)]$^+$, and lowest [M(Me$_4$cyclen)(L)]$^+$ minimum energy structures, obtained using the BP86/6-311G(d,p) method, are provided in Figures S11-S13 and Tables S11-S13. The band positions in these computed IR spectra are approximations of the true band positions because of neglect of anharmonicity and approximate treatment of electron correlation in the DFT calculations. However, scaling factors for computed harmonic wavenumbers have been established for BP86 and B3LYP calculations with a basis set which is similar to the one used in this work. These are close to 1.00 (BP86, 1.0299; B3LYP, 1.0004).[76,77] Hence, the computed spectra are expected to be reasonably reliable representations of the experimental spectra.

For a given ligand (L), comparison of the spectra for [M$^+$-L], [M(Me$_4$cyclen)]$^+$, and [M(Me$_4$cyclen)(L)]$^+$ helps identify bands in [M(Me$_4$cyclen)(L)]$^+$ that arise from the [M$^+$-L], and [M(Me$_4$cyclen)]$^+$ units. For example, the IR spectra of both [M(Me$_4$cyclen)]$^+$ and **M-L-1a** [M(Me$_4$cyclen)(L)]$^+$ show an intense band (at ~ 2900 cm^{-1}) and a broader group of weaker bands (within the range of 2950-3075 cm^{-1}). The 2900 cm^{-1} band corresponds to C–H stretching absorptions of both the CH_2 and CH_3 units of the Me$_4$cyclen ring. The broad band in the region 2950-3075 cm^{-1} consists of several components. The component at the highest wavenumber (~ 3050 cm^{-1}) corresponds to the C–H stretching of the CH_3 unit of the Me$_4$cyclen ring and in the case of the **M-L-1a** structures (L = THF, DEE, DCM), this band is also associated with the C–H stretching of the CH_2/CH_3 units in THF/DEE/DCM. Bands within the range 2975-3025 cm^{-1} are attributed to C–H stretching of both the CH_2 and CH_3 units of the Me$_4$cyclen ring and in the case of the **M-THF-1a** (M = Li, Na, K) and **M-DEE-1a** (M = Li, Na) structures, they also correspond to the C–H stretching vibrations of the CH_2/CH_3 units of THF/DEE.

The computed IR spectra of the lowest [M(Me$_4$cyclen)]$^+$ minimum energy structures in the C–H stretching region are very similar to those of the [M(Me$_4$cyclen)(L)]$^+$ structures, except for the presence of additional band(s) due to L in the case of **M-L-1a** structures (L =

THF, DEE, MeOH). An additional band at around 2940 cm^{-1} due to C–H stretching in THF is observed in the IR spectra of the **M-THF-1a** structures. Further, two additional weak bands due to C–H stretching in CH_2 (~ 2960 cm^{-1}) and CH_3 (~ 2970 cm^{-1}) units in DEE are observed in the IR spectra of the **M-DEE-1a** structures (M = Li, Na). On the other hand, for the **K-DEE-1a** structure, where DEE adopts a TT configuration, the C–H stretching of CH_2 (~ 2910 and 2945 cm^{-1}) and CH_3 (~ 2960 cm^{-1}) units of DEE are associated with three additional bands. In the case of the **M-MeOH-1a** structures, two additional bands due to C–H stretching of the CH_3 unit in MeOH are observed at around 2950 and 3060 cm^{-1}.

Other new bands are seen in the $[M(Me_4cyclen)(L)]^+$ spectra which are not present in the $[M^+\text{-}L]$, and $[M(Me_4cyclen)]^+$ units and these occur in the low wavenumber region below 500 cm^{-1}. For example, for $[M(Me_4cyclen)(L)]^+$ with L = THF, metal-oxygen (M–O) stretching modes are computed at 413, 219, and 176 cm^{-1} and for L = MeOH, these modes occur at 452, 244, and 183 cm^{-1}.

These spectra should be valuable to help confirm the presence and establish the structure of the $[M(Me_4cyclen)(L)]^+$ complex ions when they are made experimentally. More details of the computed spectra are given in the SI.

3.4 Bond Dissociation Energies (BDEs)

BDEs for the process $[M(Me_4cyclen)(L)]^+ \rightarrow [M(Me_4cyclen)]^+ + L$ were calculated using the DFT method with the BP86 and B3LYP functionals and the 6-311G(d,p) basis set. More reliable values were obtained using high level single-point DF-LCCSD(T) and DF-LCCSD(T)-F12x calculations at the BP86 and B3LYP optimised geometries. The calculated BP86 and the corresponding DF-LCCSD(T) and DF-LCCSD(T)-F12x BDEs for BP86 **M-L-1a** minimum energy structures are presented in Table 2 while BDEs derived for the B3LYP **M-L-2a** minimum energy structures are shown in Table S14. The BDE values obtained will provide insight into the choice of appropriate solvent/s to be used for the synthesis of the **M-L-1a** (**M-L-2a**) complexes and may further aid in controlling the product composition (*via* removal/addition of appropriate solvents which are Lewis bases).[24] As can be seen in Tables 2 and S14, the BP86 and B3LYP BDEs are consistent, with the B3LYP BDEs being always slightly higher than the BP86 values. The single-point higher level calculations provide more reliable BDEs than the DFT values. The DF-LCCSD(T) and DF-

LCCSD(T)-F12x BDEs, obtained using both the double and triple-ζ quality basis sets, are comparable to each other. However, they are significantly higher than the BSSE corrected DFT BDE values, with differences in the region of 6-40 kJ.mol^{-1} being observed.

Table 2: Calculated bond dissociation energies (kJ.mol^{-1}) of the lowest **M-L-1a** minimum energy structures.

	BP86/6-311G(d,p)		DF-LCCSD(T)/nZ //BP86/6-311G(d,p)		DF-LCCSD(T)-F12x[a]/nZ-F12 //BP86/6-311G(d,p)			
					n = D		n = T	
	ΔE^{ZPE}	$\Delta E^{ZPE+BSSE}$	n = D	n = T	x = a	x = b	x = a	x = b
Li-H_2O-1a	64.3	39.7	56.6	59.1	59.3	59.5	60.1	60.3
Li-THF-1a	56.3	43.1	71.6	74.3	76.8	77.3	77.2	77.4
Li-DEE-1a	34.3	21.6	67.3	57.9	59.7	60.2	61.7	61.9
Li-MeOH-1a	58.0	40.1	60.0	64.0	64.8	65.1	65.6	65.8
Li-DCM-1a	12.6	6.6	32.6	32.1	33.6	33.9	34.2	34.4
Na-H_2O-1a	67.2	45.3	51.1	57.5	55.5	55.7	57.5	57.6
Na-THF-1a	63.9	52.1	64.6	67.0	70.6	70.8	70.6	70.7
Na-DEE-1a	46.4	35.1	50.0	52.7	56.4	56.7	55.7	55.8
Na-MeOH-1a	62.2	46.5	56.5	60.2	60.0	60.1	59.6	59.5
Na-DCM-1a	21.7	15.8	38.2	39.5	40.2	40.5	39.3	39.3
K-H_2O-1a	55.0	39.0	42.1	43.0	43.7	43.8	45.3	45.5
K-THF-1a	52.8	44.2	53.3	50.0	51.2	51.1	51.1	51.3
K-DEE-1a	39.7	31.1	54.4	51.4	51.1	51.1	53.4	53.5
K-MeOH-1a	49.9	38.4	45.3	45.5	45.3	45.2	46.9	47.0
K-DCM-1a	19.4	15.5	32.6	32.8	31.5	31.5	33.2	33.3

[a] The 3*A ansatz in conjunction with the (Fix,NoX) options was used; the MOLPRO default option is (Loc,Fix).

The **M-DCM-1a** (**M-DCM-2a**) structures have lower BDEs than their *O*-containing analogues. These lower BDEs are representative of the weak interaction between DCM and [M(Me$_4$cyclen)]$^+$ and this correlates with the M–Cl bond distances in the DCM complexes being much longer than the M–O bond distances in the *O*-donor ligand complexes (Table 1). This is also consistent with the fact that DCM was used during the synthesis of the alkali metal-Me$_4$cyclen complexes, [Li(Me$_4$cyclen)(H$_2$O)][BAr^F] and [Na(Me$_4$cyclen)(THF)][BAr^F], but was not incorporated as a ligand into the product crystals

obtained. For M = Li and Na, the **M-L-1a** (**M-L-2a**) structures have DF-LCCSD(T) and DF-LCCSD(T)-F12x BDEs in the order of L = THF > MeOH > DEE ≈ H_2O, with the strongest interaction being between THF and $[M(Me_4cyclen)]^+$. The BSSE uncorrected DFT BDEs do not follow the same trend, although the BSSE corrected values do, and this indicates the importance of BSSE correction in calculating DFT BDEs. Higher level calculations based on the BP86 lowest minimum energy structures show that the BDEs of **K-THF-1a** and **K-DEE-1a** are comparable, while those based on the B3LYP lowest minimum energy structures show that the BDE for **K-DEE-2a** is marginally greater than that of **K-THF-2a**. The trend in the DFT BDEs for the loss of *O*-donor ligands from **K-L-1a** (**K-L-2a**) is not consistent with that obtained from the higher level calculations which are in the order of THF ≈ DEE > MeOH > H_2O. The DFT BDEs for the loss of L from the $[M^+$-L] structures follow a similar trend (L = THF > DEE > MeOH > H_2O > DCM; see Table S5) as that for the **K-L-1a** (**K-L-2a**) structures. The BDE values, obtained using the higher level calculations, decrease on going from $Li^+ \rightarrow Na^+ \rightarrow K^+$ for **M-L-1a** (**M-L-2a**) for a given L, where L = H_2O, THF, DEE, and MeOH, consistent with the lengthening of the M–O bond. However, the DFT BDEs do not follow the same trend. At all levels of theory, the BDEs of **Na-DCM-1a** (**Na-DCM-2a**) are higher than that of the Li^+ analogues. The bidentate η^2-Cl,Cl coordination mode between DCM and $[Na(Me_4cyclen)]^+$ in **Na-DCM-1a** (**Na-DCM-2a**) corresponds to a stronger interaction compared to the monodentate η^1-Cl coordination mode between DCM and $[Li(Me_4cyclen)]^+$ in **Li-DCM-1a** (**Li-DCM-2a**). The BDEs of **K-DCM-1a** (**K-DCM-2a**) are lower than their Li^+ and Na^+ counterparts at the DF-LCCSD(T) and DF-LCCSD(T)-F12x methods, though with marginal differences between the BDE values of **M-DCM-1a** (**M-DCM-2a**), for M = Li and K. In contrast, the DFT BDEs for the dissociation process, $[M^+$-DCM] $\rightarrow M^+$ + DCM, decrease systematically on going from $Li^+ \rightarrow Na^+ \rightarrow K^+$ (Table S5).

As already has been mentioned, the default (Loc,Fix) ansatz option in MOLPRO yields reasonable BDEs for all $[M(Me_4cyclen)(L)]^+$ complexes, for M = Li, Na, and K, except for L = DCM. The problem is associated with the way Cl atoms are treated with this ansatz option. The (Fix,NoX) ansatz option does not suffer from this problem. The (Fix,NoX) option is therefore recommended and it was employed in all the DF-LCCSD(T)-F12x/nZ-F12x calculations for the purposes of investigating basis set effects. The dependence of the

calculated BDEs on the methods and basis sets used in this work are depicted in Figures S15 and S16 (with relevant BDE values provided in Tables 2 and S14). The ansatz options to be used for the DF-LCCSD(T)-F12x calculations and the basis set effects on the DF-LCCSD(T) and DF-LCCSD(T)-F12x calculations are discussed further in the SI.

The main conclusions of this section are:-

(i) The geometry effects on the BDEs from the two functionals used are negligibly small.

(ii) In DF-LCCSD(T)-F12x calculations with MOLPRO, the (Fix,NoX) ansatz option is necessary, as the default (Loc,Fix) option gives rise to errors in relative energies for chlorine-containing molecules.

(iii) Calculations with the DF-LCCSD(T) method with a DZ basis set are inadequate, but DF-LCCSD(T)-F12x calculations with a DZ-F12 basis set are expected to be reliable and give accurate relative energies. This latter method is recommended for calculations of BDEs for the type of complexes considered in this work.

In summary, for lower level geometry optimisation calculations, some commonly used functionals, such as BP86 or B3LYP, used in the present study, appear to be adequate, while for improved relative electronic energies, the DF-LCCSD(T)-F12x method with basis sets of at least DZ-F12 quality is required, though it is noted that the (Fix,NoX) ansatz option should be employed in the DF-LCCSD(T)-F12x calculations instead of the default (Loc,Fix) option.

Table 2 clearly shows (e.g. for the DF-LCCSD(T)-F12x/DZ-F12//BP86/6-311G(d,p) values) for the **M-L-1a** complexes (BP86 geometries) that for a given metal, M = Li, Na, or K, the BDE is lowest when L = DCM. Also, for a given ligand, the BDE is lowest when M = K. The same trends are observed in Table S14 for **M-L-2a** complexes (B3LYP geometries).

4.0 Conclusions

This work, to study the structure and bonding in $[M(Me_4cyclen)(L)]^+$ complexes, was initiated by results of an experimental study which prepared some Group 1 metal cyclen complexes, namely $[Li(Me_4cyclen)(H_2O)][BAr^F]$ and $[Na(Me_4cyclen)(THF)][BAr^F]$ and obtained their X-ray crystal structures.[22] This experimental work was notable in that although reactions were carried out in DCM as the solvent (in presence of some H_2O or THF), no DCM was incorporated into the $[M(Me_4cyclen)(L)]^+$ product ions in the crystals obtained.

Also, attempts to synthesise the corresponding K^+ (and Rb^+ and Cs^+) complexes failed and resulted in the formation of the [Me_4cyclenH][BAr^F].

To investigate this and to understand the role of commonly used solvents, L, the DFT method was employed to study the [M(Me_4cyclen)(L)]$^+$ complexes, where M = Li, Na, K, and L = H_2O, THF, DEE, MeOH, DCM. Coordination of L to the [M(Me_4cyclen)]$^+$ fragment entails small though systematic changes in their respective optimised geometries. H_2O, THF, DEE, and MeOH bind to the M^+ centre (for Li, Na, and K) in a monodentate η^1-O coordination mode while DCM interacts in both monodentate η^1-Cl (for Li) and bidentate η^2-Cl,Cl (for Na and K) coordination modes. Computed geometrical parameters for [Li(Me_4cyclen)(H_2O)]$^+$ and [Na(Me_4cyclen)(THF)]$^+$ are compared with those derived from available crystal structures[22] and good agreement was obtained. Bonding analysis shows that the complexes are stabilised *via* mostly ionic interaction with electron density transfer from the L and Me_4cyclen ligands to mainly the vacant 2s, 3s, and 4s orbitals of Li^+, Na^+, and K^+, respectively. Single-point DF-LCCSD(T) and the explicitly correlated DF-LCCSD(T)-F12x calculations were employed to obtain accurate bond dissociation energy (BDE) for the loss of the L from [M(Me_4cyclen)(L)]$^+$. The DF-LCCSD(T)-F12x calculations were performed (using MOLPRO) with the 3*A ansatz in conjunction with two different options, namely (Fix,NoX) and (Loc,Fix). The ansatz option (Loc,Fix) performs poorly for *Cl*-containing species. BDEs derived from both sets of ansatz options for the loss of *O*-donor ligands are consistent not only with each other but also with the results obtained using the DF-LCCSD(T) method. The DCM molecule is weakly bound to the [M(Me_4cyclen)]$^+$ fragment compared to the *O*-donor analogues. This is consistent with the available experimental evidence that even when DCM is used as a solvent, in the presence of THF or H_2O, in the preparation of [M(Me_4cyclen)(L)]$^+$ complexes, DCM is not present in the [M(Me_4cyclen)(L)]$^+$ ion obtained in the crystalline product. The [M(Me_4cyclen)(L)]$^+$ complexes (M = Li, Na) have BDEs in the order of THF > MeOH > DEE ≈ H_2O, while those of their K^+ analogues are in the order of THF ≈ DEE > MeOH > H_2O, with the strongest interaction being between THF and [M(Me_4cyclen)]$^+$. The BDE associated with the loss of L is lowest for the K^+ complexes and this is consistent with the unsuccessful syntheses of [M(Me_4cyclen)(L)]$^+$ complexes containing potassium. In short, for M = K the ionic bonding in [M(Me_4cyclen)(L)]$^+$ is not sufficiently large to favour formation of [K(Me_4cyclen)(L)]$^+$

over formation of $[Me_4cyclenH]^+$. Further, coordinating ligands L (such as acetonitrile, benzene, pentane, chloroform, 2-propanol, and pyridine) in $[M(Me_4cyclen)(L)]^+$ are currently being investigated.

5.0 Acknowledgements

The authors acknowledge the use of the EPSRC UK National Service for Computational Chemistry Software. This work was also supported by funding provided by the Tertiary Education Commission of Mauritius (TEC). Helpful advice from Profs Bill Levason and Gill Reid (University of Southampton) is also acknowledged.

6.0 References

1. Y. Kim, T.-T. T. Nguyen, and D. G. Churchill, *In: The Alkali Metal Ions: Their Role for Life*; A. Sigel, H. Sigel, and R. K. O. Sigel, Eds., *Met. Ions Life Sci.*, Springer International Publishing, **16**, 2016, 1.
2. G. R. C. Hamilton, S. K. Sahoo, S. Kamila, N. Singh, N. Kaur, B. W. Hylanda, and J. F. Callan, *Chem. Soc. Rev*. 2015, **44**, 4415.
3. M. C.-L. Yeung and V. W.-W. Yam, *Chem. Soc. Rev*. 2015, **44**, 4192.
4. C. J. Pedersen, *J. Am. Chem. Soc*. 1967, **89**, 7017.
5. Y. El Aziz, P. G. Taylor, A. R. Bassindale, S. J. Coles, and M. B. Pitak, *Organometallics* 2016, **35**, 4004.
6. I. V. Kolesnichenko and E. V. Anslyn, *Chem. Soc. Rev*. 2017, **46**, 2385.
7. L. Moreira, B. M. Illescas, and N. Martín, *J. Org. Chem*. 2017, **82**, 3347.
8. J. Li, D. Yim, W.-D. Jang, and J. Yoon, *Chem. Soc. Rev*. 2017, **46**, 2437.
9. R. B. Nazarski, *In: Macrocyclic Chemistry: New Research Development*; D. W. Fitzpatrick and H. J. Ulrich, Eds., Nova Science Publishers Inc.: New York, 2010, 1.
10. S. Shinoda, *Chem. Soc. Rev*. 2013, **42**, 1825.
11. K. Hanaoka, K. Sasakura, Y. Suwanai, S. Toma-Fukai, K. Shimamoto, Y. Takano, N. Shibuya, T. Terai, T. Komatsu, T. Ueno, Y. Ogasawara, Y. Tsuchiya, Y. Watanabe, H. Kimura, C. Wang, M. Uchiyama, H. Kojima, T. Okabe, Y. Urano, T. Shimizu, and T. Nagano, *Sci. Rep*. 2017, **7**, 40227.
12. L. Wang, H. Lin, L. Ma, J. Jin, T. Shen, R. Wei, X. Wang, H. Ai, Z. Chen, and J. Gao, *Nanoscale* 2017, **9**, 4516.
13. E. M. Surender, S. J. Bradberry, S. A. Bright, C. P. McCoy, D. C. Williams, and T. Gunnlaugsson, *J. Am. Chem. Soc.* 2017, **139**, 381.
14. T. Sagami, Y. O. Tahara, M. Miyata, H. Miyakea, and S. Shinoda, *Chem. Comm*. 2017, **53**, 3967.
15. S. Buøen, J. Dale, P. Groth, and J. Krane, *J. Chem. Soc., Chem. Comm*. 1982, 1172.

16. K. Igarashi, T. Nogamia, and T. Ishida, *J. Chem. Soc. Chem., Comm*. 2007, 501.
17. S. Standfuss, T. P. Spaniol, and J. Okuda, *Eur. J. Inorg. Chem*. 2010, 2987.
18. H. Ito, H. Tsukube, and S. Shinoda, *Chem. Eur. J*. 2013, **19,** 3330 and references therein.
19. H. Ito and S. Shinoda, *Chemistry Open* 2014, **3**, 238 and references therein.
20. X. Zhang, J. Yin, and J. Yoon, *Chem. Rev*. 2014, **114**, 4918.
21. E. Kriemen, M. Holzapfel, E. Ruf, J. Rehbein, and W. Maison, *Eur. J. Inorg. Chem*. 2015, 5368.
22. J. M. Dyke, W. Levason, M. E. Light, D. Pugh, G. Reid, H. Bhakhoa, P. Ramasami, and L. Rhyman, *Dalton Trans*. 2015, 13853.
23. H. Bhakhoa, L. Rhyman, E. P. F. Lee, P. Ramasami, and J. M. Dyke, *Chem. Eur. J*. 2016, **22**, 4469.
24. A. Causero, G. Ballmann, J. Pahl, H. Zijlstra, C. Färber, and S. Harder, *Organometallics*, 2016, **35**, 3350.
25. H.-J. Werner and M. Schütz, *J. Chem. Phys*. 2011, **135**, 144116.
26. T. B. Adler and H.-J. Werner, *J. Chem. Phys*. 2011, **135**, 144117.
27. A. J. Achazi, L. K. S. v. Krbek, C. A. Schalley, and B. Paulus, *J. Comput. Chem*. 2016, **37**, 18.
28. E. Goll, T. Leininger, F. R. Manby, A. Mitrushchenkov, H.-J. Werner, and H. Stoll *Phys. Chem. Chem. Phys.* 2008, **10**, 3353.
29. J. P. Perdew, *Phys. Rev. B* 1986, **33**, 8822.
30. P. J. Stephens, F. J. Devlin, C. F. Chabalowski, and M. J. Frisch, *J. Phys. Chem*. 1994, **98**, 11623.
31. H. B. Schlegel, *J. Comput. Chem*. 1982, **3**, 214-218.
32. H. B. Schlegel, *In: Modern Electronic Structure Theory*; D. R. Yarkony, Ed., World Scientific Publishing: Singapore, 1995, 459.
33. W. J. Hehre, L. Radom, P. v. R. Schleyer, and J. Pople, *Ab Initio Molecular Orbital Theory*; Wiley: New York, 1986.
34. M. J. D. Champion, J. M. Dyke, W. Levason, M. E. Light, D. Pugh, H. Bhakhoa, L. Rhyman, P. Ramasami, and G. Reid, *Inorg. Chem*. 2015, **54**, 2497.
35. C. Adamo and V. Barone, *J. Chem. Phys.* 1999, **110**, 6158.
36. S. F. Boys and F. Bernardi, *Mol. Phys*. 1970, **19**, 553.
37. M. J. Frisch *et al.*, *Gaussian 09*, Revision D.01, Gaussian, Inc., Wallingford CT, 2009.
38. A. E. Reed, R. B. Weinstock, and F. Weinhold, *J. Chem. Phys*. 1985, **83**, 735.
39. A. E. Reed, L. A. Curtiss, and F. Weinhold, *Chem. Rev*. 1988, **88**, 899.
40. E. D. Glendening, A. E. Reed, J. E. Carpenter, and F. Weinhold, NBO Version 3.1, 2001, University of Wisconsin-Madison.
41. MOLPRO, version 2015.1, a package of *ab initio* programs, H.-J. Werner, P. J. Knowles, G. Knizia, F. R. Manby, M. Schütz, and others, see http://www.molpro.net.
42. R. Polly, H.-J. Werner, F. R. Manby, and P. J. Knowles, *Mol. Phys*. 2004, **102**, 2311.
43. H.-J. Werner, T. B. Adler, and F. R. Manby, *J. Chem. Phys*. 2007, **126**, 164102.
44. G. Knizia and H.-J. Werner, *J. Chem. Phys*. 2008, **128**, 154103.

45. https://www.molpro.net/info/2015.1/doc/manual/node462.html.
46. T. H. Dunning, Jr., *J. Chem. Phys*. 1989, **90,** 1007.
47. D. E. Woon and T. H. Dunning, Jr, *J. Chem. Phys*. 1993, **98**, 1358.
48. R. A. Kendall, T. H. Dunning, Jr., and R. J. Harrison, *J. Chem. Phys*. 1992, **96,** 6796.
49. F. Weigend, A. Köhn, and C. Hättig, Efficient *J. Chem. Phys*. 2002, **116**, 3175.
50. C. Hättig *Phys. Chem. Chem. Phys*. 2005, **7**, 59.
51. F. Weigend, *Phys. Chem. Chem. Phys.* 2002, **4**, 4285.
52. http://www.molpro.net/info/basis.php?version=current&describe=1&element=O&basis=aug-cc-pVDZ-JKFI
53. K. A. Peterson, T. Adler, and H.-J. Werner, *J. Chem. Phys*. 2008, **128,** 084102.
54. K. E. Yousaf and K. A. Peterson, *J. Chem. Phys*. 2008, **129**, 184108.
55. B. Prascher, D. E. Woon, K. A. Peterson, T. H. Dunning, Jr., and A. K. Wilson, *Theor. Chem. Acc.* 2011, **128**, 69.
56. J. G. Hill and K. A. Peterson, *Phys. Chem. Chem. Phys*. 2010, **12**, 10460.
57. F. Weigend, *J. Comput. Chem*. 2008, **29**, 167.
58. F. Weigend and R. Ahlrichs, *Phys. Chem. Chem. Phys*. 2005, **7**, 3297.
59. V. Navrátil, V. Klusák, and L. Rulíšek, *Chem. Eur. J*. 2013, **19**, 16634.
60. F. Weigend, M. Häser, H. Patzelt, and R. Ahlrichs, *Chem. Phys. Lett*. 1998, **294**, 143.
61. http://www.molpro.net/info/basis.php?version=current&describe=1&element=H&basis=def2-TZVPP-MP2FI
62. A. Hellweg, C. Hättig, S. Höfener, and W. Klopper, *Theor. Chem. Acc*. 2007, **117**, 587.
63. G. Knizia, Dissertation, 2010; http://www.molpro.net/info/basis.php?version=current&describe=1&element=Cl&basis=def2-TZVPP_OPT
64. I. S. Lim, P. Schwerdtfeger, B. Metz, and H. Stoll, *J. Chem. Phys*. 2005, **122**, 104103.
65. http://www.molpro.net/info/basis.php?version=current&describe=1&element=K&basis=ECP10MDF
66. R. Dooley, K. Milfeld, C. Guiang, S. Pamidighantam, and G. Allen, *J. Comput. Sci*. 2014, **5**, 576.
67. N. Shen, Y. Fan, and S. Pamidighantam, *J. Comput. Sci.* 2014, **5**, 576.
68. This work used the Extreme Science and Engineering Discovery Environment (XSEDE), which is supported by National Science Foundation grant number OCI-1053575.
69. R. D. Shannon, *Acta Crystallogr., Sect. A: Cryst. Phys., Diffr., Theor. Gen. Cryst*. 1976, **32**, 751.
70. N. Kuze, N. Kuroki, H. Takeuchi, T. Egawa, and S. Konaka, *J. Mol. Struct*. 1993, **301**, 81.
71. N. Kuze, E. Kojima, H. Fujiwara, H. Takeuchi, T. Egawa, and S. Konaka, *J. Mol. Struct*. 1996, **375**, 231.

72. M. Mantina, A. C. Chamberlin, R. Valero, C. J. Cramer, and D. G. Truhlar, *J. Phys. Chem. A* 2009, **113**, 5806.
73. K. Kimura, S. Katsumata, Y. Achiba, T. Yamazaki, and S. Iwata, *Handbook of HeI Photoelectron Spectra of Fundamental Organic Molecules. Ionization Energies, Ab Initio Assignments, and Valence Electronic Structure for 200 Molecules,* Halsted, New York, 1981.
74. J. E. Huheey, *Inorganic Chemistry: Principles of Structure and Reactivity*, New York, Harper & Row, 1983.
75. A. Decken, C. Knapp, G. B. Nikiforov, J. Passmore, J. M. Rautiainen, X. Wang, and X. Zeng, *Chem. Eur. J.* 2009, **15**, 6504.
76. M. K. Kesharwai, B. Brauer, and J. M. L. Martin, *J. Phys. Chem. A* 2015, **119**, 1701.
77. I. M. Alecu, J. Zheng, Y. Zhao, and D. G. Truhlar, *J. Chem. Theory Comput*. 2010, **6**, 2872.